Effect of reduced graphene oxide on the properties of an activated carbon cloth/polyaniline flexible electrode for supercapacitor application

Ming Zhong [a,b], Yan Song [a,*], Yongfeng Li [a,b], Chang Ma [a,b], Xiaoling Zhai [a,b], Jingli Shi [a], Quangui Guo [a,**], Lang Liu [a]

[a] Key Laboratory of Carbon Material, Institute of Coal Chemistry, Chinese Academy of Science, Taiyuan 030001, China
[b] Graduate University of the Chinese Academy of Science, Beijing 100049, China

HIGHLIGHTS

► Interfacial interaction of ACC/PANI is improved by the addition of RGO.
► Charge transfer property of ACC/PANI is improved by the addition of RGO.
► Compared to ACC/PANI, ACC/RGO/PANI shows better electrochemical properties.

GRAPHICAL ABSTRACT
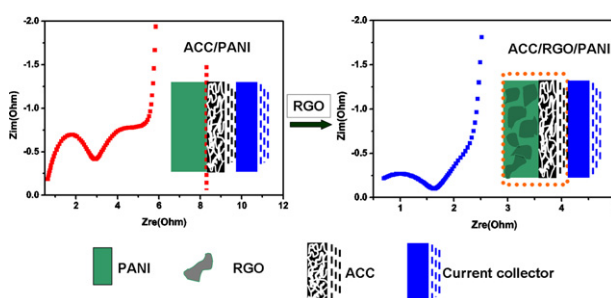
ARTICLE INFO

ABSTRACT

Reduced graphene oxide (RGO) is synthesized and added in situ into the reaction system of polyaniline (PANI) electrodeposition using activated carbon cloth (ACC) as the substrate. The effect of RGO on the morphology, structure, and electrochemical properties of the ACC/PANI composite is investigated. A more compact and uniform layer of PANI film is observed via scanning electronic microscopy after the addition of RGO. Raman spectroscopy shows that RGO has been simultaneously deposited with PANI onto the surface of ACC. X-ray photoelectron spectroscopy reveals that the sample with RGO exhibits a higher sulfur-to-nitrogen ratio. The reversibility of the redox reaction of PANI is improved, as confirmed via cyclic voltammetry. The electrochemical impedance spectroscopy data shows that the introduction of RGO lowers the charge-transfer resistance of ACC/PANI, meanwhile, improves the coverage percentage of PANI on the ACC surface to a significant extent, primarily because of the interactions between RGO, ACC, and PANI. The as-prepared composite with RGO shows improved rate performance and cyclability as a supercapacitor electrode.

1. Introduction

Supercapacitors have drawn considerable attention because of their high power density, long cycle life, and potential application in electric vehicles, consumer electronics, and other devices [1,2].

Electrode materials play an important role in the performance of supercapacitors. Porous carbon materials [3,4] are extensively used as electrode materials for supercapacitors because of their large surface areas and good conductivity. However, the energy density and specific capacitances of porous carbon materials are relatively low, which is unfavorable for micromation in electronic devices. To resolve this problem, several researchers studied the composites of porous carbon and transition metal oxides or conducting polymers that provide a pseudocapacitance [5–7]. However, the new interface between two phases may hamper the charge transfer when

* Corresponding author. Tel.: +86 355 4250553; fax: +86 355 4083952.
** Corresponding author. Tel.: +86 355 4084106.
E-mail addresses: yansong1026@126.com (Y. Song), qgguo@sxicc.ac.cn (Q. Guo).

these composites are fabricated. To the best of our knowledge, although several reports have concentrated on the effect of the interfaces between the current collector and the composite or between the composite and the electrolyte on different kinds of electronic devices [8,9], few studies have focused on the charge-transfer resistance of the composite itself as well as the interface between the two components.

Graphene, which is a single-layer graphite with close-packed conjugated hexagonal lattices, is recognized as the basic building block of all dimensional graphitic materials. Its unique structure endows graphene with various superior properties such as high electrical conductivity and charge-carrier mobility, good transparency, high mechanical strength, inherent flexibility, and large specific surface area. Therefore, graphene has attracted much attention during recent years in the fields of microelectronic and optoelectronic devices, energy storage materials, electrocatalysts, polymer composites, and ultrastrong paper-like materials [10]. Pure single-layer graphene is difficult to prepare in large amounts, and the typical product is usually in the form of reduced graphene oxide (RGO). RGO not only has good electrical properties and a large conjugated aromatic ring structure similar to that of graphene, which can physically interact with porous carbon materials, but also has many functional groups that can chemically interact with conducting polymers. Based on the interface formation and semiconductor electronic theories [11,12], enhancing the physical and chemical interactions between two phases decreases the energy gap width between the conduction and valence bands of the composite, which is beneficial for charge transfer.

Compared with conventional powder materials, self-forming electrode materials such as films and felts are more attractive because they have continuous current path thereby decreasing the interparticle resistance. In the current work, an activated carbon cloth (ACC) with a specific surface area of 2084 $m^2 g^{-1}$ is used as the porous carbon substrate because of its flexibility [13]. Polyaniline (PANI), which is more competitive than metal oxides when combined with RGO [14], is deposited onto the ACC surface via a potentiostatic method. RGO is dispersed into the reaction system during electrochemical deposition in an aqueous medium containing H_2SO_4 to improve the interfacial interaction and charge-transfer property of ACC/PANI. Scanning electron microscopy (SEM), Raman spectroscopy, X-ray photoelectron spectroscopy (XPS), cyclic voltammetry (CV), electrochemical impedance spectroscopy (EIS), and galvanostatic techniques are used to investigate the effect of RGO on the morphology, structure, and electrochemical properties of the as-prepared ACC/PANI composite samples.

2. Experimental

2.1. Synthesis

GO was prepared from natural graphite (20019128, Sinopharm Chemical Reagent Co. Ltd, Shanghai, China) using a modified Hummers method [15]. RGO was produced via chemical reduction according to literature [16]. In a typical process, GO (0.15 g) in 150 ml water was sonicated and 1.35 g *p*-phenylene diamine (PPD) was dissolved in 150 ml N,N-dimethylformamide. The colloid and the solution were mixed and refluxed in a water bath at 90 °C for 24 h. After filtration and washing with acetone, the RGO powder was transferred into ethanol. Afterward, a stable RGO colloid in ethanol, denoted as GE, was formed via mild ultrasonication. The RGO concentration in the GE colloid was 2 mg ml^{-1}.

Aniline was distilled with zinc powder under a nitrogen atmosphere at reduced pressure. The resulting colorless liquid was kept in the dark at 0 °C. An electrochemical cell was assembled in a three-electrode configuration, in which the counter electrode was platinum (Pt), the reference electrode was a saturated calomel electrode (SCE), and the working electrode was ACC with a fiber diameter of approximately 10 μm (type 507-20, Kynol, Japan; 0.30 μm thickness). The total deposition area of the ACC was 7.5 cm^2, with an area density of 66 g/m^2, and the separation between Pt and ACC was 2 cm. ACC was attached to a Pt foil using graphite emulsion (Xiyou Graphite Co. Ltd., Qingdao, China) as an adhesive. A 50 ml electrolyte solution of 1 M H_2SO_4 and 0.05 M aniline was used for the electrochemical deposition of PANI on the ACC electrode. The deposition of PANI was conducted at a constant potential of 0.90 V for 1500 s at 30 °C. Subsequent to deposition, the electrode was washed with distilled water and dried in a vacuum oven overnight at 60 °C. This sample was denoted as ACC/PANI. On the other hand, the sample designated as ACC/RGO/PANI was synthesized using the same procedure long extended for ACC/PANI, with the addition of 5 ml GE into the electrolyte. Compared with ACC substrate, the weight increase of ACC/PANI and ACC/RGO/PANI is 9.28 mg and 16.65 mg, respectively.

2.2. General characterization of the composites

The surface characteristics were recorded via XPS using Thermo ESCALAB 250. The XPS spectra were recorded using an Al Kα (hv = 1486.6 eV) irradiation as the photon source, with a power density of 150 W and a pass energy of 20 eV. The surface morphology was observed via SEM (JEOL JSM6700LV). The Raman spectrum was taken on a JY Labram HR800 Raman microscope using a 532 nm excitation to analyze the scattered light from the sample surface. The laser power was kept low at approximately 0.1 mW to avoid sample burning. All spectra were recorded from 400 cm^{-1} to 1700 cm^{-1}. The microstructure of RGO was analyzed using high-resolution transmission electron microscopy (HR-TEM, JEOL, JEM-2100) and X-ray diffraction (XRD, Bruker D8) spectroscopy.

2.3. Electrochemical measurements

Electrochemical measurements of the samples were performed on a CHI 660C instrument (Shanghai Chenhua, China) using a three-electrode system at ambient temperature and 1 M H_2SO_4 as the electrolyte solution. A Pt foil and SCE served as the counter and the reference electrodes, respectively. The working electrode was activated species attached to a Pt foil using graphite emulsion. The weights of activated species such as ACC, ACC/PANI, and ACC/RGO/PANI were 2.54, 3.10, and 3.40 mg, respectively. CV and galvanostatic charge−discharge measurements of the electrodes were performed in the 0−0.7 V potential range *vs.* SCE. EIS was conducted at the bias potential of 0.5 V with potential amplitude of ac 5 mV and the frequency ranging from 10^5 Hz to 10^{-2} Hz.

3. Results and discussion

The SEM images of the samples with and without RGO are shown in Fig. 1. A PANI layer is clearly formed in Fig. 1a, compared with the smooth surface of ACC shown in Fig. S1a. The product without RGO is more loose and porous (Fig. 1a). The exfoliation degree is sufficiently high based on the TEM image of RGO (Fig. S1b). The RGO nanosheets are stacked after drying in air (Fig. S1c). The XRD pattern (Fig. S2) is in good agreement with previously reported results [16] and the carbon-to-oxygen ratio is 5.7 (Table S1), indicating that RGO has indeed been fabricated. When RGO is introduced, a compact and uniform film appears without a trace of pores (Fig. 1b). In addition, the film is not smooth but has a considerable number of microgrooves, which may be
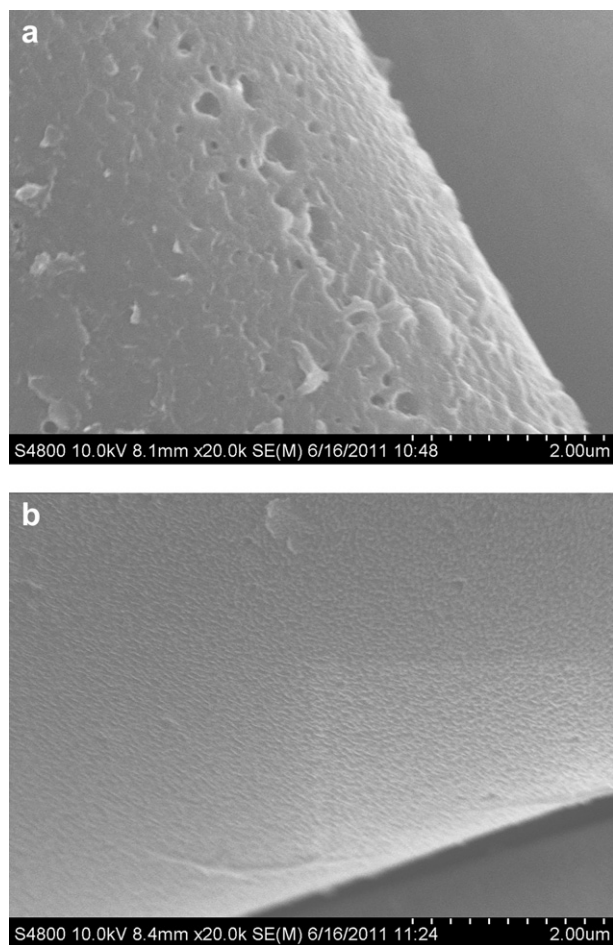
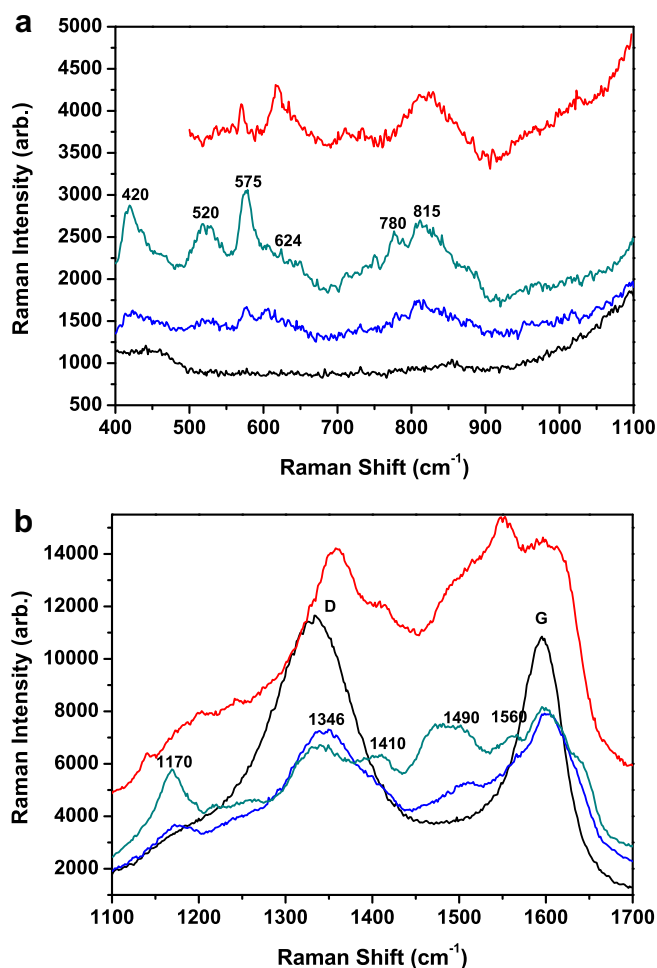**Fig. 1.** SEM images of (a) ACC/PANI and (b) ACC/RGO/PANI.

Fig. 2. Raman spectra of ACC (black), RGO (red), ACC/PANI (blue), and ACC/RGO/PANI (olive). [For interpretation of color in this figure legend, the reader is referred to web version of the article.]

attributed to a successful incorporation of RGO into PANI matrix on the ACC surface.

Raman spectroscopy is used to confirm the existence of RGO deposition on the ACC surface together with PANI. The Raman spectra of ACC, RGO, ACC/PANI, and ACC/RGO/PANI at low and high wavenumber regions are presented in Fig. 2a and b without further smoothening. ACC/PANI and ACC/RGO/PANI show the same spectra at low wavenumber regions but with different peak intensities and sharpness. The band at around 420 cm^{-1} can be attributed to out-of-plane amine ring deformations, whereas the band near 520 cm^{-1} corresponds to in-plane amine ring deformations. Ring deformation and phenazine- or phenoxazine-like segments are identified by the bands at around 575 and 624 cm^{-1}. The peaks at 780 and 815 cm^{-1} correspond to imine and amine deformation (C–N–C bending), respectively [17,18]. In Fig. 2b, the Raman spectra of pure ACC and RGO show very distinctive peaks for the *D* (1348 cm^{-1}) and *G* (1598 cm^{-1}) bands. The *G* band represents the in-plane bond-stretching motion of the C sp^2 atom pairs (the E_{2g} phonons), whereas the *D* band corresponds to the breathing modes of the rings or the *K*-point phonons of A_{1g} symmetry [19]. The peaks at 1410 and 1560 cm^{-1} are ascribed to phenazine- or phenoxazine-like segments [20]. The C–H bending mode in the benzene- or quinone-type rings is centered at around 1170 cm^{-1}. C–N$^+$ stretching at around 1346 cm^{-1} and C=N stretching vibration in the emeraldine base of imines at approximately 1490 cm^{-1} are observed, revealing the presence of the PANI structures [21]. Compared with ACC/PANI, the ACC/RGO/PANI composite presents

a shift of the C–N$^+$ stretching peak toward low wavenumbers because of π–π interaction between RGO and the PANI molecules.

The phenazine- or phenoxazine-like segments in the RGO structure is possibly due to the reaction between GO and PPD. The presence of the bands at 1410 and 1560 cm^{-1}, which derives from RGO, are detected in ACC/RGO/PANI, indicating that RGO is indeed incorporated in the PANI matrix.

XPS is used to investigate the different electronic structures of ACC/PANI and ACC/RGO/PANI. The C 1s core-level spectra of ACC/PANI and ACC/RGO/PANI are presented in Fig. 3. The C 1s XPS spectrum is deconvoluted into five subpeaks, which are related to aromatic C–H (284.62 eV), C–C/C–N/C=N/C=N$^+$ (285.91 eV), C–N$^+$/C=O (287.5 eV), O–C–O (289.01 eV), and O–C=O (291.06 eV) [16,22]. Compared with ACC/PANI (Fig. 3a), all five peak locations for ACC/RGO/PANI (Fig. 3b) shift toward a lower binding energy (BE), which is presumably due to a better conductivity in the surface of ACC/RGO/PANI. Better conductivity is likely to cancel a positive charge build-up which is caused by a loss of photoelectrons during the XPS measurement. The C 1s deconvolution results of the relative atomic concentrations are listed in Table 1. After the addition of RGO, the increase in the atomic concentrations of C–C, C–N, C=N, and C=N$^+$ at 285.55 eV and of C–N$^+$ and C–O at 296.95 eV from 26.0% to 51.2% and 4.3–15.8%, respectively, further confirms that RGO, which possesses a certain amount of C–C, C=N, C–N, and C–O bonds [16], has been

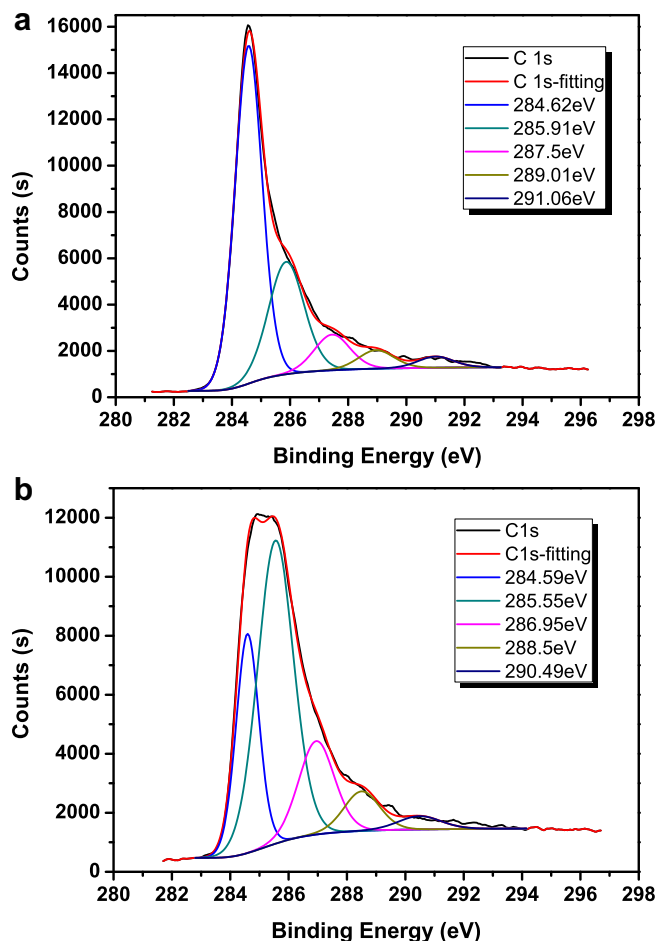**Fig. 3.** C 1s XP spectra for (a) ACC/PANI and (b) ACC/RGO/PANI.

Fig. 4. N 1s XPS spectra of (a) ACC/PANI and (b) ACC/RGO/PANI.

successful incorporated into PANI matrix. This result is consistent with that of the Raman analysis. The atomic concentration of the aromatic C−H decreases from 58.9% to 23.6%, owing to the introduction of RGO who contains a large area of aromatic and conjugated structures.

Fig. 4a shows that the deconvolution of the N 1s core-level spectrum of ACC/PANI results in three peaks correlated to three different electronic states, namely, the quinoid imine with BE at 399.77 eV, the benzenoid amine with BE centered at 400.73 eV, and the nitrogen cationic radical (N^+) with BE at 402.5 eV. Given the existence of ACC, the BE values are higher than that reported in literature for a graphene/PANI composite [23]. On the other hand, these three different ACC/RGO/PANI electronic states are also observed without a peak shift (Fig. 4b), suggesting that RGO has negligible effect on the chemical environments of the nitrogen atoms in the PANI molecular chains.

In addition, a fourth ACC/RGO/PANI electronic state is observed at 404.18 eV. At present, the ascription of this state remains unclear; however, this finding has no apparent effect on the conclusion of
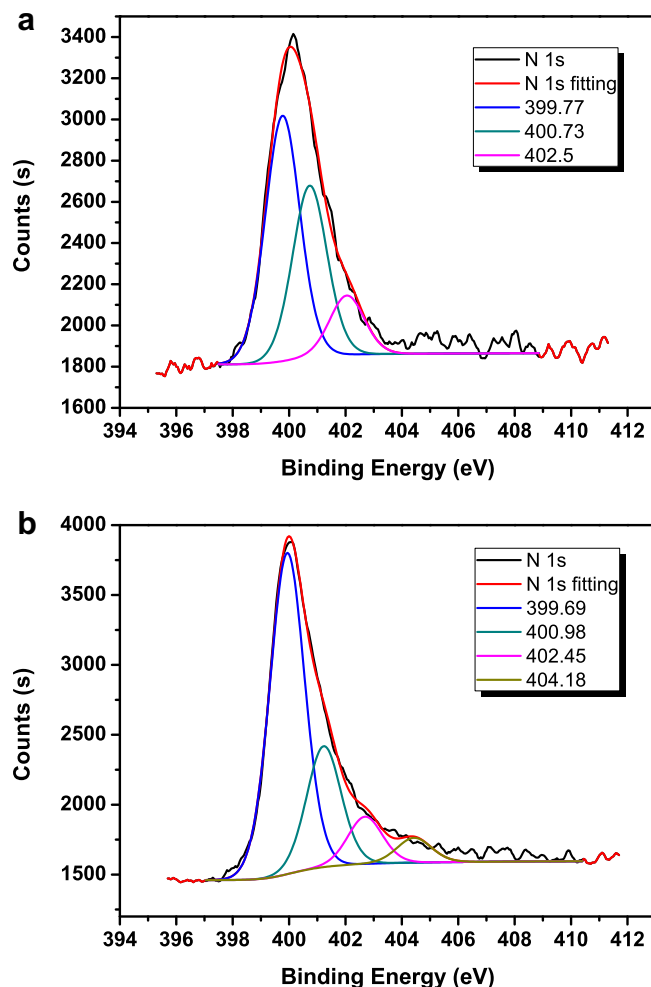
the present research. The obvious change in the atomic nitrogen concentration from 51.5% to 62.5% at 399.93 eV, and from 36.1% to 23.5% at 401.35 eV, as shown in Table 1, indicates that the quantity of the quinoid imine structure in PANI increases, implying the enhanced extent of PANI oxidation. RGO, which has a considerable number of active points, may act as a catalyst during electrochemical oxidation of aniline. The results of the elemental chemical composition as determined by XPS are given in Table S1. The carbon content in ACC/RGO/PANI decreases because of the increase in the amount of the other elements. The sulfur-to-nitrogen ratio is related to the level of doping and the conductivity of sulfated PANI [24,25]. The value changes from 0.195 for ACC/PANI to 0.213 for ACC/RGO/PANI. However, the value of RGO is just 0.153 (Table S1), so it can be concluded that PANI in ACC/RGO/PANI shows better conductivity than that in ACC/PANI.

The potential of using these composites as electrode materials for supercapacitors is tested via standard cyclic voltammetry. The

Table 1
C 1s and N 1s deconvolution results of the relative atomic concentrations (%).

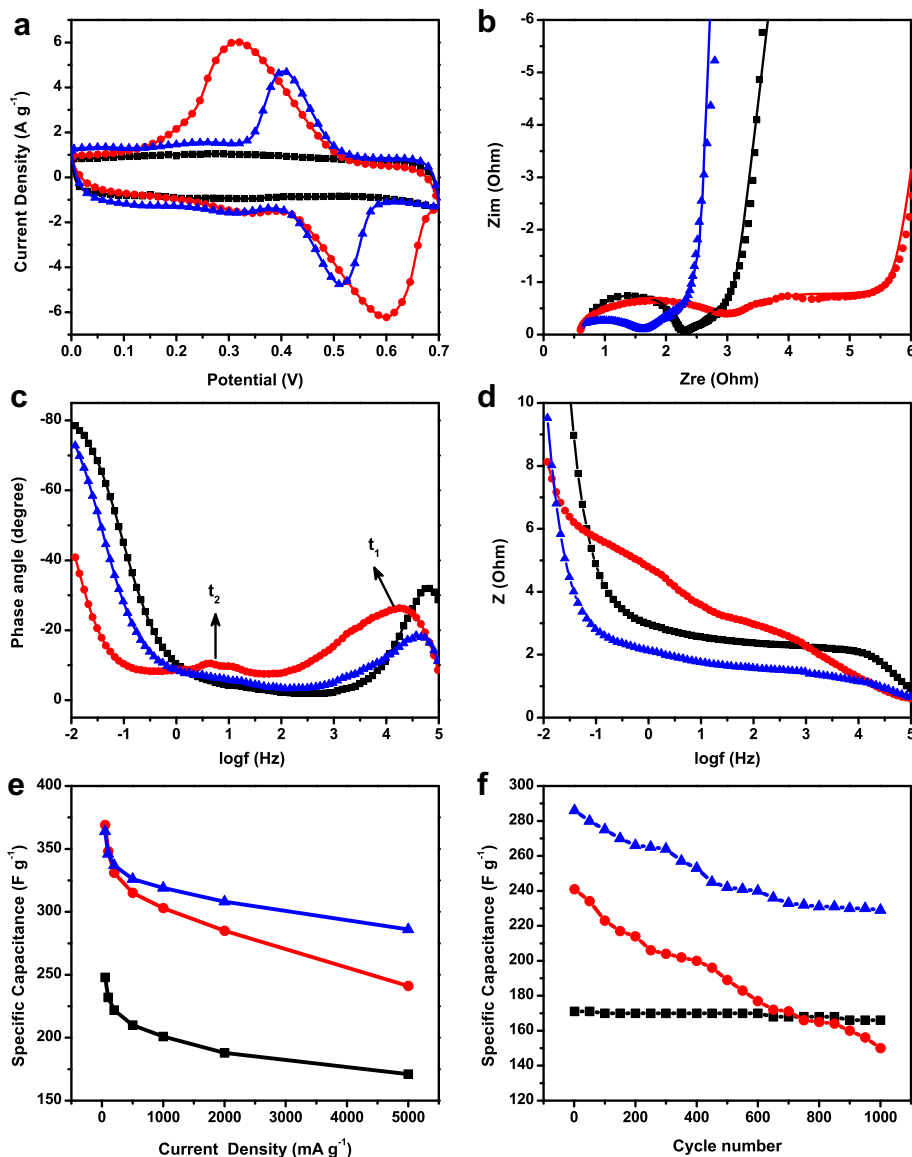| samples	C 1s (atom%)					N 1s (atom%)			
	Aromatic C−H	C−C/C−N/C=N/C=N^+	C−N^+/C−O	O−C−O	O−C=O	=N−	−NH−	N^+	Not clear
ACC/PANI	58.9	26.0	4.3	2.6	8.2	51.5	36.1	12.4	−
ACC/RGO/PANI	23.6	51.2	15.8	6.7	2.7	62.5	23.5	9.2	4.8

Fig. 5. (a) Electrochemical properties of ACC (black), ACC/PANI (red), and ACC/RGO/PANI (blue). (b) Nyquist diagrams of the experimental (scattering dot) and fitting results (solid line). [For interpretation of color in this figure legend, the reader is referred to web version of the article.]

cyclic voltammograms of the two different electrodes within a potential window from 0 V to 0.7 V (*vs.* SCE) and at a scan rate of 5 mV s^{-1} are shown in Fig. 5a. The current signal is immediately reversed upon the reversal of the potential sweep, indicating the low resistance of the device [26]. The potential difference ($\Delta E_{a,c}$) between the anodic and cathodic peaks is used as a measure of the reversibility of the electrochemical redox reaction, that is, the higher the reversibility, the smaller the $\Delta E_{a,c}$ [27]. The redox reaction of PANI in ACC/RGO/PANI is more reversible than that of ACC/PANI.

The electrode materials with lower resistance in the supercapacitors are electrochemically preferred primarily as power devices for better applicability. The complex-plane impedance plots of the two electrodes in the 10^{-2} Hz to 10^{5} Hz frequency range, derived from the EIS and conducted at bias potentials of 0.5 V with an ac perturbation of 5 mV, are shown in Fig. S3. The partially enlarged view of Fig. S3 is given in Fig. 5b. The Nyquist plot of ACC displays a small semicircle at high frequency, followed by a transition to linearity at low frequency, which is the typical feature of activated carbon. Interestingly, two semicircles are observed for

ACC/PANI, which is probably due to the poor contact at the phase interface between ACC and PANI in the composite, as illustrated in the left sketch in Fig. 6. However, only one semicircle appears in the ACC/RGO/PANI curve. The semicircle is closely related to the
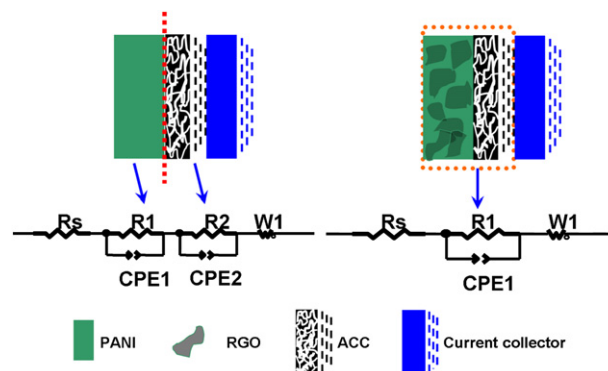

Fig. 6. Electric equivalent circuits of ACC/PANI (left) and ACC/RGO/PANI (right).

electron-transfer process and the electrical conductivity of the electrode material. For ACC/RGO/PANI, the radius of the semicircle decreases to almost one-third of that of the ACC/PANI electrode, indicating a dramatic reduction in the polarization resistance. The EIS results are fitted using the Zview software, and the equivalent circuits are given in Fig. 6. The values of the circuit components are listed in Table 2. Chi-square, which is a measure of the quality of the fit, shows that the fitting results are acceptable. Furthermore, the equivalent series resistance [28] (ESR = R_s+R_1+R_2) decreases from 4.97 Ω to 1.63 Ω after the addition of RGO, which is in agreement with the cyclic voltammogram results. The constant phase element (CPE)-T is related to the surface fractal dimension structure [29]. The smaller the CPE-P, the rougher the surface. The CPE-P values are in good agreement with the SEM analysis. The diffusion parameter W−P with regard to the finite diffusion characteristic is nearly 0.5 [30]. Both the diffusion resistance W−R and the diffusion time W−T become smaller for ACC/RGO/PANI because of the good conductivity of RGO.

The bode plots are shown in Fig. 5c and d. The phase angle of ACC/PANI observed at low frequency is nearly −40°, whereas that of ACC/RGO/PANI is nearly −90°, which indicates a better capacitive response. At the intermediate frequency, the phase angle shifts to 0° and remains constant over a wide range of frequencies, indicating nearly similar resistance responses for all the materials. ACC/PANI has two time constants, which is consistent with the equivalent circuit of the Nyquist plot illustrated by the left sketch in Fig. 6 and with the other report showing two RC circuits [31]. This finding indicates that another state variable exists aside from the electrode potential. The second state variable is believed to be the coverage percentage of ACC by PANI [32]. Regarding ACC/PANI the relatively poor coverage percentage results in two semicircles in its Nyquist plot. On the other hand, one time constant for ACC/RGO/PANI suggests that the electrode potential is the only state variable, implying that the ACC surface has been completely covered by PANI and RGO. The time constant of ACC/RGO/PANI is 6 μs, which is smaller than that of ACC/PANI (74 μs) and indicates a higher charge and discharge rate [33]. After PANI is deposited onto the ACC surface, the number of time constants increases from one to two. However, when RGO nanosheets are simultaneously deposited with PANI, the second time constant disappears, revealing that the coverage percentage at the electron-transfer interface between ACC and PANI has been dramatically improved because of the possible interaction after RGO addition. Given the higher coverage percentage in ACC/RGO/PANI, only one semicircle at high frequency is shown in the Nyquist plot.

Fig. 5d shows that ACC/RGO/PAIN has the lowest impedance value among the three samples. Both composites have higher specific capacitances than pure ACC (Fig. 5e) because of the redox

pseudocapacitance of PANI. The difference in ESR affects the rate performance of the supercapacitor [34]. The specific capacitance of the ACC/PANI electrode decreases from 369 F g^{-1} to 241 F g^{-1} as the current density increases from 50 mA g^{-1} to 5000 mA g^{-1}, indicating a capacitance loss of approximately 35%. This poor rate performance is ascribed to the low electrical conductivity of ACC/PANI, as well as its long diffusion time and large electron-transfer resistance. On the other hand, a capacitance loss of approximately 21% is observed as the current density increases from 50 mA g^{-1} to 5000 mA g^{-1} for the ACC/RGO/PANI electrode. The cyclability of the electrode is also tested via continuous charge−discharge measurement in a 1 mol L^{-1} H_2SO_4 electrolyte. Fig. 5f shows the performance of the different electrodes measured at a current density of 5 A g^{-1} in a three-electrode cell. For the ACC/RGO/PANI electrode, the specific capacitance gradually decreases during the first 500 cycles, and then remains stable with further increase in the cycle number. Approximately 80% specific capacitance is preserved after 1000 galvanostatic charge−discharge cycles, showing the better cyclability of ACC/RGP/PANI compared with that of ACC/PANI, whose specific capacitance continuously decreases to 60% of the initial value, which is even lower than that of ACC.

The better electrochemical performance of ACC/RGO/PANI is ascribed to its structure, which has improved bond−bond interactions (Fig. 7). First, because there are aromatic rings of graphene [35] and oxygen-containing groups on the ACC surface, the RGO nanosheets can attach to ACC through hydrogen bonding and π−π stacking. Given the conjugated structure in larger areas and the presence of certain residual oxygen-containing groups of RGO, the density and intensity of the interactions between RGO and ACC are stronger than those between PANI and ACC. This feature is beneficial for the electron transfer on the interface. Second, apart from π−π stacking, electrostatic interactions, and hydrogen-bonding interactions between the PANI molecular chains and the RGO nanosheets [36], the RGO nanosheets could link with the PANI molecular chains through other covalent bonds. It has been proved by earlier literature that the phenazine- or phenoxazine-like segments in the RGO nanosheets found in the Raman spectra can exist in the backbone of PANI chains [37−39] or form copolymer with PANI [40], implying that the phenazine- or phenoxazine-like segments can react with aniline or aniline oligomers to form covalent bonds. This kind of covalent link reduces the electron-transfer resistance between different PANI molecular chains. The higher intensity and density interaction between the RGO nanosheets and ACC, the covalent bonds and other interactions with PANI molecular chains, as well as its high conductivity, make RGO nanosheets suitable for reducing the interfacial resistance between ACC and PANI. In addition, the RGO nanosheets overlap one other, possibly to form a conductive network through sheet plane contact [41], which also facilitates the fast electron transfer between PANI and ACC. All these factors lead to the smaller charge-transfer resistance of ACC/PANI and enhances the coverage percentage of

Table 2
Values of the equivalent circuit elements obtained by fitting the experimental results in the Nyquist diagrams represented in Figure S3.

Samples	ACC	ACC/PANI	ACC/RGO/PANI
Rs/Ω	0.61646	0.49308	0.33818
R1/Ω	1.651	2.372	1.29
CPE1-T[a]/F	6.8956E−6	0.00072557	0.0023792
CPE1-P	0.9324	0.65016	0.49714
R2/Ω	−	2.101	−
CPE2-T/F	−	0.074403	−
CPE2-P	−	0.61776	−
W1-R[b]/Ω	2.42	2.355	2.287
W1-T/s	1.141	5.747	3.173
W1-P	0.46856	0.46689	0.47493
Square of Chi/ × 10^{-3}	2.1	2.1	3.9

[a] CPE represents the constant phase element and is defined by two values, CPE-T and CPE-P.
[b] W represents the Warburg diffusion impedance and is related to R, T, and P.
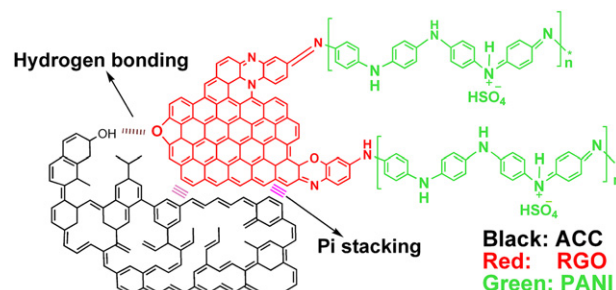

Fig. 7. Interactions between ACC and PANI after the addition of RGO.

ACC. RGO facilitates the integration of PANI with ACC, as shown in the right sketch in Fig. 6.

4. Conclusions

In the current work, RGO nanosheets are dispersed into the PANI electropolymerization reaction system. PANI is then deposited onto the ACC surface. The characterization results confirm that the RGO nanosheets have been successfully deposited onto the ACC surface with PANI. By contrast, the addition of RGO nanosheets promotes the oxidation and doping degree of PANI, forms a conductive network through sheet plane contact, and enhances the interfacial interaction. As a result, better electrochemical performance, such as higher electron conductivity, increased reversibility of PANI redox reaction, better rate performance, longer cycle life, and smaller charge-transfer resistance are obtained. RGO may have a potential application in reducing the charge-transfer resistance of various composites for electrode materials.

Acknowledgements

Appendix A. Supplementary material

Supplementary material associated with this article can be found, in the online version, at http://dx.doi.org/10.1016/j.jpowsour.2012.05.086.

References

[1] L.L. Zhang, X.S. Zhao, Chemical Society Reviews 38 (2009) 2520–2531.
[2] M. Jayalakshmi, K. Balasubramanian, International Journal of Electrochemical Science 3 (2008) 1196–1217.
[3] A.G. Pandolfo, A.F. Hollenkamp, Journal of Power Sources 157 (2006) 11–27.
[4] M. Inagaki, H. Konno, O. Tanaike, Journal of Power Sources 195 (2010) 7880–7903.
[5] D.S. Su, R. Schlogl, Chemsuschem 3 (2010) 136–168.
[6] M. Toupin, T. Brousse, D. Bélanger, Chemistry of Materials 16 (2004) 3184–3190.
[7] Y.-G. Wang, H.-Q. Li, Y.-Y. Xia, Advanced Materials 18 (2006) 2619–2623.
[8] S. Yoshihara, H. Katsuta, H. Isozumi, M. Kasai, K. Oyaizu, H. Nishide, Journal of Power Sources 196 (2011) 7806–7811.
[9] K. Hanai, M. Ueno, N. Imanishi, A. Hirano, O. Yamamoto, Y. Takeda, Journal of Power Sources 196 (2011) 6756–6761.
[10] Y.Q. Sun, Q.O. Wu, G.Q. Shi, Energy & Environmental Science 4 (2011) 1113–1132.
[11] F.Z. Hu, Materials Surface and Interface, East China University of Science and Technology Press, Shanghai, 2008, pp. 151–156.
[12] W.Y.Z.A. Hu, Solid Physics Science, Higher Education Press, Beijing, 2006, pp. 229–266.
[13] Y. Geng, Y. Song, M. Zhong, J. Shi, Q. Guo, L. Liu, Materials Letters 64 (2010) 2673–2675.
[14] A.K. Mishra, S. Ramaprabhu, The Journal of Physical Chemistry C 115 (2011) 14006–14013.
[15] W.S. Hummers, R.E. Offeman, Journal of the American Chemical Society 80 (1958) 1339.
[16] Y. Chen, X. Zhang, P. Yu, Y. Ma, Chemical Communications (2009) 4527–4529.
[17] M. Jain, S. Annapoorni, Synthetic Metals 160 (2010) 1727–1732.
[18] R. Mazeikiene, A. Statino, Z. Kuodis, G. Niaura, A. Malinauskas, Electrochemistry Communications 8 (2006) 1082–1086.
[19] J. Yan, T. Wei, B. Shao, Z. Fan, W. Qian, M. Zhang, F. Wei, Carbon 48 (2010) 487–493.
[20] M. Trchová, E.N. Konyushenko, J. Stejskal, J. Kovárová, G. Ciric-Marjanovic, Polymer Degradation and Stability 94 (2009) 929–938.
[21] M. Cochet, G. Louarn, S. Quillard, J.P. Buisson, S. Lefrant, Journal of Raman Spectroscopy 31 (2000) 1041–1049.
[22] A.A. Qaiser, M.M. Hyland, D.A. Patterson, The Journal of Physical Chemistry B 115 (2011) 1652–1661.
[23] K. Zhang, L.L. Zhang, X.S. Zhao, J. Wu, Chemistry of Materials 22 (2010) 1392–1401.
[24] X.L. Wei, Y.Z. Wang, S.M. Long, C. Bobeczko, A.J. Epstein, Journal of the American Chemical Society 118 (1996) 2545–2555.
[25] M. Pyo, J.-H. Hwang, Synthetic Metals 159 (2009) 700–704.
[26] G. Wee, O. Larsson, M. Srinivasan, M. Berggren, X. Crispin, S. Mhaisalkar, Advanced Functional Materials 20 (2010) 4344–4350.
[27] Z. Gao, J. Wang, Z. Li, W. Yang, B. Wang, M. Hou, Y. He, Q. Liu, T. Mann, P. Yang, M. Zhang, L. Liu, Chemistry of Materials 23 (2011) 3509–3516.
[28] C.-T. Hsieh, S.-M. Hsu, J.-Y. Lin, H. Teng, The Journal of Physical Chemistry C 115 (2011) 12367–12374.
[29] C.M.A. Brett, A.M.O. Brett, Electrochemistry, Principles, Methods and Applications, Oxford University Press, London, 1993.
[30] H. Farsi, F. Gobal, H. Raissi, S. Moghiminia, Journal of Solid State Electrochemistry 14 (2009) 643–650.
[31] Y.-Y. Horng, Y.-C. Lu, Y.-K. Hsu, C.-C. Chen, L.-C. Chen, K.-H. Chen, Journal of Power Sources 195 (2010) 4418–4422.
[32] Y. Zheng, J.M. Wang, H. Chen, J.Q. Zhang, C.N. Cao, Materials Chemistry and Physics 84 (2004) 99–106.
[33] P. Sivaraman, V.R. Hande, V.S. Mishra, C.S. Rao, A.B. Samui, Journal of Power Sources 124 (2003) 351–354.
[34] Z. Lei, N. Christov, X.S. Zhao, Energy & Environmental Science 4 (2011) 1866–1873.
[35] R.L.-R. Paola E. Diaz-Flores, Jose R. Rangel-Mendez, Mariana Michel Ortiz, Rosa M. Guerrero-Coronado, Jovita Mendoza-Barron, Journal of Environmental Engineering and Management 16 (2006) 249–257.
[36] H. Wang, Q. Hao, X. Yang, L. Lu, X. Wang, ACS Applied Materials & Interfaces 2 (2010) 821–828.
[37] J. Stejskal, M. Trchová, Polymer International 61 (2012) 240–251.
[38] J. Stejskal, I. Sapurina, M. Trchová, E.N. Konyushenko, P. Holler, Polymer 47 (2006) 8253–8262.
[39] M. Trchová, I. Šenková, E.N. Konyushenko, J. Stejskal, P. Holler, G. Ćirić-Marjanovi&cacute, The Journal of Physical Chemistry B 110 (2006) 9461–9468.
[40] N. Boutaleb, A. Benyoucef, H.J. Salavagione, M. Belbachir, E. Morallón, European Polymer Journal 42 (2006) 733–739.
[41] H. Gómez, M.K. Ram, F. Alvi, P. Villalba, E. Stefanakos, A. Kumar, Journal of Power Sources 196 (2011) 4102–4108.